JOURNAL OF PROPULSION AND POWER
Vol. 16, No. 5, September–October 2000

Prediction of the Dissipation of a Solid-Rocket Contrail

Eugene Miller*
Mackay School of Mines, University of Nevada, Reno, Nevada 89557

Starting with predictions of solid-propellant-rocket plume-gas temperatures and compositions, and secondary smoke droplet properties from literature cited computer programs, a new model of the dissipation of a rocket contrail is presented. Equations describing the growth and evaporation of the secondary smoke droplets comprising the contrail with time and plume location are given. Gravity settling of the droplets, the change of gas temperature and composition with time by diffusion, and the initial location of the droplets in the plume control the contrail dissipation. An example is given for a typical 87 wt % ammonium perchlorate, 1 wt % aluminum, and 12 wt % rubber binder solid-propellant (reduced smoke) rocket flying horizontally at 200 ft/s through air at sea level, 22°C, and 96% relative humidity.

Nomenclature

C_p, c_p	= specific heat per unit mole and mass, respectively, at constant pressure
c	= number concentration per unit volume
D	= mass diffusivity
H_c, H_s	= heat of condensation and solution per unit mass, respectively
k	= Boltzmann constant, mass-transfer coefficient, thermal conductivity
L	= gas mean free path
Le	= Lewis Number
M	= molecular weight, relaxation parameter
m	= mass of droplet
N	= number of droplets collected per unit time by a cloud of falling droplets
P	= total pressure
Pr	= Prandtl Number
PSI	= streamline coordinate from LAPP program
p	= partial pressure of condensable in plume
$\bar{p}$	= saturation vapor pressure of component of plane surface solution
p_r	= equilibrium vapor pressure of the droplet
R	= gas constant, mean droplet radius
r	= droplet radius
Sc	= Schmidt Number
T	= absolute temperature
t	= time
v	= specific volume per mole
v	= droplet Stokes settling velocity
x	= unit distance
YR	= plume radial distance from centerline
Z	= axial distance
α	= thermal diffusivity
γ	= specific heat ratio
ε	= capture coefficient
μ	= gas absolute viscosity
ν	= gas kinematic viscosity
ρ	= gas density
σ	= surface tension of the liquid-gas interface
τ	= time increment
Φ	= transport factor

Subscripts

B	= stagnant gas
d	= mass
f	= film
h	= heat
i	= ith component
lm	= log mean
p	= pressure
r	= droplet
t	= time

Introduction

PLUMES emitting from reduced smoke and minimum smoke solid-propellant rocket motors contain significant quantities of water and hydrogen chloride gases or water, respectively. Smoke may form anywhere in the plume in the form of droplets where the thermodynamic dew-point requirements of temperature and composition are met. Such smoke is termed secondary smoke to differentiate it from primary smoke in the form of solid alumina, other metal oxides, carbon, liner debris, etc. Oliver[1] first predicted from thermodynamic considerations the ambient temperature and relative humidity for which secondary smoke could form for the cases of isothermal and adiabatic mixing of the plume with the air. Oliver's method permitted an estimate of the climatic conditions for which secondary smoke might form but did not quantify its density, visibility, or the attenuation of an optical beam passing through the plume. These aspects of secondary smoke and a description of experimental tools for predicting and quantifying the formation of visible secondary-smoke contrails were the subject of several papers by Miller,[2–4] Hoshizaki et al.,[5] Victor and Breil,[6] and Victor.[7]

Subsequent to motor shutdown, the rocket contrail persists. Problems of interference of the contrails with optical guidance systems, visibility of the launch platform, obscuration of the battlefield, contamination of onboard optical systems, and possible health hazards to personnel remain. The present paper is concerned with modeling the disappearance of the contrail and predicting how long the contrail will persist as a function of the plume properties and atmospheric conditions—the model being termed CONDIS. An example is given for a typical 87 wt % ammonium perchlorate, 1 wt % aluminum, and 12 wt % rubber-binder reduced-smoke solid-propellant rocket flying at 200 ft/s through the air at one atmosphere pressure, 22°C, and 96% relative humidity.

Analysis

A description for this example of the mean secondary-smoke droplet radius as a function of its radial and axial position in the plume during motor operation, as predicted by the DROP[2] program, is given in Fig. 1. The rocket plume was modeled by the

Received 19 October 1998; revision received 15 July 1999; accepted for publication 16 August 1999.

*Professor Emeritus, Chemical and Metallurgical Engineering Department; emiller@scs.unr.edu.

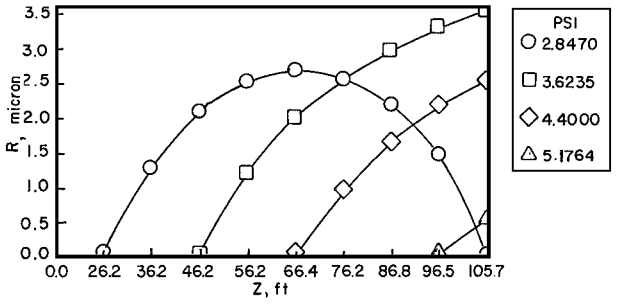

Fig. 1 Predicted plume secondary-smoke-droplet mean radius as a function of streamline and axial locations.

LAPP[8] plume program, defining radially and axially the gas velocity, mass concentrations, and temperature fields. The LAPP program is based on free shear-layer mixing with nonequilibrium chemistry. As described in Ref. 2, the radial mass concentrations of water and HCl predicted by the LAPP program were modified semi-empirically—the correction being small for water but large for the HCl concentration profile. PSI values given in the figure are streamline coordinates used in the LAPP program. Although visually the secondary smoke in the rocket plume appears to be a continuum, in actuality, as may be seen in the figure, along a streamline in general droplets grow by condensation and then ultimately evaporate. It is the multiplicity of streamline droplet growths and evaporation that give the appearance of uniformity. Secondary smoke forms along the outermost streamlines in the plume boundary layer as the temperature decreases, and the HCl and water concentrations increase to a state that permits condensation on heterogeneous nuclei. The radii of the condensation nuclei vary from $0.1000E-02$ to 0.1200μ with a size distribution depending on the particular type of propellant. In this example, only nuclei with radii equal to or larger than 0.061μ grow by condensation. The droplets start on a given streamline with a range of sizes, but they rapidly grow to a uniform maximum size and subsequently evaporate uniformly. Details of nucleation of condensation, the nuclei concentration, the size distribution of the droplets formed, and the corrections to the LAPP concentration profiles are given in Ref. 2. HCl concentration in the droplets vary with axial and radial location. Condensation is exaggerated in ammonium perchlorate formulations because the presence of HCl in the exhaust gases depresses the equilibrium vapor pressure of water leading to increased condensation. Computer models of droplet formation during motor operation have been described in detail previously in the aforementioned references.

The rate at which a droplet will grow or evaporate may be written as

$$\frac{dr}{dt} = \frac{\Phi_d v_r D_f (p - p_r)}{RT_f r(1 - p_r)} \tag{1}$$

where Φ_d is given by

$$\Phi_d = \frac{2\left(1.0 + 0.3\sqrt{Re_f}\sqrt[3]{Sc_f}\right)}{\left(\sqrt{2\pi M/RT_r}\right)D\Big/r + 2r/(r + L)} \tag{1a}$$

Φ_d includes corrections for noncontinuum and nonequilibrium effects, and, in the numerator the Ranz and Marshall'[9] experimental correlation for mass transfer to spheres.

p_r is given by the Kelvin equation:

$$p_r = \bar{p}\,\exp(2\sigma v_r/RT_r) \tag{1b}$$

Analogously, the rate of temperature change in the droplet because of convective heat transfer and heats of condensation and solution is described by

$$\frac{dT_r}{dt} = \frac{4\pi\Phi_h k_f r(T - T_r) + H_c + H_s}{mc_p} \tag{2}$$

where Φ_h is defined by

$$\Phi_h = \frac{1.0 + 0.3\sqrt{Re_f}\sqrt[3]{Pr_f}}{k\sqrt{2\pi MRT_r}/[(C_p(\gamma + 1)/2\gamma)Pr + r/(r + L)]} \tag{2a}$$

The thermal accommodation and condensation coefficients have been taken as unity. The Ranz and Marshall correlation for heat transfer to spheres is included in the numerator of Eq. (2a).

The transport factors, defined in Eqs. (1a) and (2a), are dependent on the relative velocity between the droplet and the plume gases used in the Reynolds number. For the stagnant plume the relative velocity was calculated from the Stokes terminal velocity, including the Cunningham correction for slip for small droplets and the correction of the Stokes friction factor for higher Reynolds numbers for the larger droplets. As discussed in Ref. 2 in the case of the turbulent plume during motor operation the relative velocity was estimated from the turbulent energy spectrum and velocity fluctuations in the plume, the droplet radius, the ratio of droplet to gas densities, the plume velocity, and the gas turbulent viscosity.

There is no information available describing the transient behavior of the plume at motor shutoff. Here, the assumption is made that the droplet and gas properties at shutdown (time $=0$) are frozen at the values predicted by the LAPP[8] program, corresponding to a cessation of relative motion between the plume and the atmosphere. The subsequent stagnant plume is assumed, as predicted by the LAPP program, to be a circular cylinder with all of the streamlines fixed at the shutdown locations. The radial locations of the streamlines predicted by the LAPP code are independent of the axial distances chosen. Radial and axial velocities of the dynamic plume at motor shutdown are assumed to have dropped to zero. Wind or air turbulence effects on the quiescent plume are neglected.

The change in the subsequent plume temperature and composition as a function of time was predicted using the relaxation method described in Ref. 10. A rectangular grid with 20 increments was overlaid on the circular plume cross section. Fifteen increments were used for the plume itself with five additional increments external to the plume.

Briefly, the relaxation method is based on the following equations. Consider heat flow by conduction only in the x and y direction for adjacent cubical blocks of side Δx, as shown in Fig. 2:

$$k\left[(\Delta x^2/\Delta x)(t_1 + t_2 + t_3 + t_4 - 4t_0)\right]\Delta\tau = \Delta x^3\rho C_p(t_{0,\Delta\tau} - t_0) \tag{3}$$

Defining

$$M_\tau = \Delta x^2/\alpha\Delta\tau$$

where

$$\alpha = \rho C_p/k_r \tag{3a}$$

$$t_{0,\Delta\tau} = [t_1 + t_2 + t_3 + t_4 + (M_t - 4)t_0]/M_\tau \tag{3b}$$

and for $M_\tau = 5$

$$t_{0,\Delta\tau} = (t_0 + t_1 + t_2 + t_3 + t_4)/5 \tag{3c}$$

Similarly for mass transfer

$$k_p\Delta x^2[p_1 + p_2 + p_3 + p_4 - 4p_0]\Delta\tau = (p_{0,\tau} - p_0)\Delta x^3/RT \tag{4}$$

Defining

$$k_p = (PD/RT)/\Delta x p_{B,\mathrm{lm}} \tag{4a}$$

$$M_p = \Delta x^2/D\Delta t \tag{4b}$$

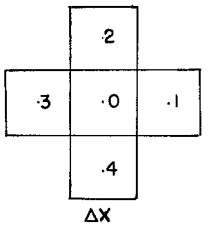

Fig. 2 Relaxation grid.

Table 1a Plume gas temperature (deg K) as a function of time and streamline coordinate PSI (axial distance = 53.67 ft)

Time, s	0	2.0706	2.8470	PSI 3.6235	4.4000	5.1764
0.00	382.8	315.4	301.0	296.1	295.2	295.2
147.6	373.3	316.9	301.8	296.6	295.3	295.2
291.6	369.9	317.1	302.2	296.8	295.4	295.2
439.2	366.6	317.2	302.5	296.9	295.4	295.2
730.8	364.2	317.3	302.8	297.0	295.4	295.2

Table 1b Plume mol fraction of water (y_{H_2O}) as a function of time and streamline coordinate PSI (axial distance = 53.67 ft)

Time, s	0	2.0706	2.8470	PSI 3.6235	4.4000	5.1764
0.00	3.307E−02	2.701E−02	2.570E−02	2.522E−02	2.511E−02	2.511E−02
147.6	3.222E−02	2.714E−02	2.577E−02	2.527E−02	2.513E−02	2.511E−02
291.6	3.191E−02	2.716E−02	2.580E−02	2.528E−02	2.513E−02	2.511E−02
439.2	3.161E−02	2.716E−02	2.583E−02	2.529E−02	2.514E−02	2.511E−02
730.8	3.119E−02	2.717E−02	2.587E−02	2.531E−02	2.514E−02	2.511E−02

Table 1c Plume mol fraction of HCl, y_{HCl}, as a function of time and streamline coordinate PSI (axial distance = 53.67 ft)

Time, s	0	2.0706	2.8470	PSI 3.6235	4.4000	5.1764
0.000	2.240E−03	8.036E−04	3.917E−04	1.455E−04	0.000E+00	0.000E+00
260.7	2.039E−03	8.203E−04	4.041E−04	1.583E−04	2.014E−05	0.000E+00
515.0	1.966E−03	8.191E−04	4.093E−04	1.605E−04	2.525E−05	0.000E+00
775.6	1.895E−03	8.171E−04	4.125E−04	1.628E−04	2.955E−05	3.498E−07
1029.9	1.843E−03	8.149E−04	4.153E−04	1.653E−04	3.337E−05	9.763E−07

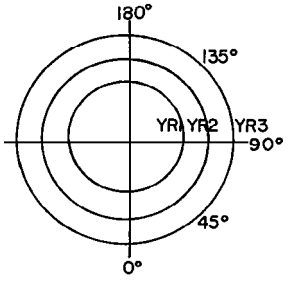

Fig. 3 Location of *YR* streamline and circumferential angle starting points of computations (not to scale).

If $P \sim p_{B,\mathrm{lm}}$,

$$p_{0,\Delta t} = [p_1 + p_2 + p_3 + p_4 + (M_p - 4)p_0]/M_p \qquad (5)$$

and as shown for M_p of 5,

$$p_{0,\Delta t} = (p_0 + p_1 + p_2 + p_3 + p_4)/5 \qquad (5a)$$

If the Lewis number $Le = \alpha/D = 1$, $M_p = M_\tau$ and the $\Delta\tau s$ for heat conduction and mass diffusion are the same. The analysis here is based on a $Le = 1$ for the diffusion of water and temperature. Because the diffusivity of HCl is significantly smaller than that of water, and its concentration is significantly less (see Table 1c, discussed later), a correction was made for the time increment for HCl by increasing it by a factor of 1.766 for the ratio of diffusivities. The use of a value of $M_p = 5$, rather than 4, provides a smaller time increment with some increase in accuracy of the predictions.

Figure 3 illustrates the cross section of the circular plume and several streamline locations, none to scale. The PSI streamlines of the LAPP program at motor shutdown (time = 0) have been replaced by their actual radial locations *YR*. Subsequent *YR* radial distances, after time zero, no longer refer to the original PSI positions. The plume is symmetrical about its centerline. Starting at the bottom of the plume cross section as 0 deg, other circumferential positions are noted for 45, 90, 135, and 180 deg. Computations were made for each of these locations for initial *YR* streamlines of 4.651, 5.692, and 6.724, and axial distances of 36.23, 56.23, 75.22, and 96.52 ft where droplets were formed in the plume.

The growth and decay of the droplets are affected by the local temperature and composition of the gases, which in turn change with time and the location of the droplets. The gas temperatures and compositions are highest in the center of the plume and decrease toward the plume edge. The growth and evaporation of the droplets in the 90–180-deg quadrant will be different from those in the 0–90-deg quadrant. Settling in the upper quadrant initially brings the droplets into higher temperatures and compositions whereas droplets in the lower quadrant will be exposed to lower temperatures and compositions. In many instances the droplets escape from the contrail into the undisturbed atmosphere in the form of rain.

Results

Typical relaxation results are illustrated for an axial distance of 53.67 ft, for gas temperature, mass fraction of water, and mass fraction of HCl as a function of time, and streamline coordinates are given in Tables 1a–1c, respectively. Gradients and variations are somewhat greater at 36.23 ft and lesser at longer axial distances, 75.22 and 96.52 ft. They are small enough that the choice of 20 Δx increments in the relaxation computation is acceptable for the contrail dissipation computations.

The results of the contrail dissipation computations are summarized in Tables 2a–2c. At each axial distance in feet and circumferential position, deg, R, μ, and *YR*, ft are given for t(init) or 0 s, t(max), time to maximum droplet radius, and t(end), time for the droplet to evaporate totally to its condensation nucleus radius.

Effect of Initial Circumferential Position

0, 45, and 90 deg

At the 36.23-ft axial distance the mean droplet radius grows from the initial *YR* at 4.65 ft relatively quickly and then evaporates more slowly to the nucleus by the time it settles to the edge of the plume. A similar behavior is found for the outermost *YR* streamlines at axial distances 56.23, 75.22, and 96.52 ft, although at the longest distance the final nucleus radius of 0.061μ is reached much further

out from the original plume edge and after some 225 s at 45 deg. At the inner *YR* streamlines for 56.23 ft and greater axial distances, the maximum droplet radius is developed outside the original plume radius and finally evaporates to the nucleus at distances far removed from the plume edge. At 90 deg the droplet behavior is not too different except that the maximum droplet size develops over longer time periods.

180 deg

In contrast to the droplet growth and evaporation pattern found at 0 and 45 deg, for all *YR* and axial distance values the droplets grow to smaller maxima quickly and evaporate completely within the plume in less than 2.8 s. This occurs because all of the droplets are falling into higher temperature fields where the effect of temperature overrides that of the increased condensable gas concentration. Typical plots of droplet radius vs time, initial circumferential position, and *YR* are shown in Figs. 4 and 5.

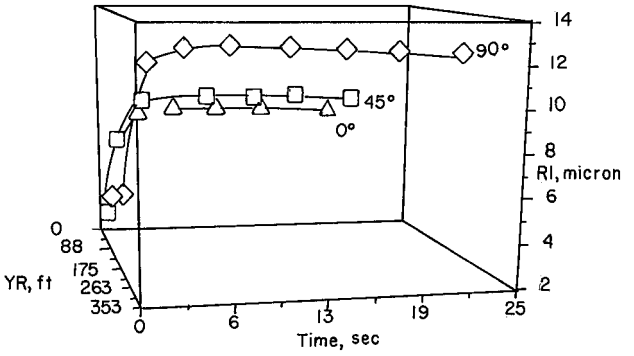

Fig. 4 Predicted droplet mean radius as a function of *YR* (starting at 4.65 ft), time, and starting circumferential angles (0, 45, and 90 deg) at an axial distance of 56.23 ft.

Table 2a *R* and *YR* as a function of time, axial distance, and starting circumferential angles 180 and 0 deg

			180 deg				0 deg	
Z/angle, ft	Second	*R*1/*YR*1, μm/ft	*R*2/*YR*2, μm/ft	*R*3/*YR*3, μm/ft	Second	*R*1/*YR*1, μm/ft	*R*2/*YR*2, μm/ft	*R*3/*YR*3, μm/ft
36.23	*t*(init) 0.00	1.28/4.65	——	——	0.00	1.28/4.65	——	——
	t(max) 0.93	4.91/4.05	——	——	1.21	2.04/4.95	——	——
	t(end) 1.65	0.061/2.65	——	——	23.7	0.061/7.85	——	——
56.23	*t*(init) 0.00	2.52/4.65	1.22/5.69	——	0.00	2.52/4.65	1.22/5.69	——
	t(max) 0.85	4.76/3.09	——	——	5.83	8.63/27.3	——	——
	1.99	——	4.81/3.03	——	1.10	——	1.84/5.92	——
	t(end) 1.99	0.061/3.02	——	——	346.1	0.061/798	——	——
	2.05	——	0.061/2.97	——	32.8	——	0.061/7.97	——
75.22	*t*(init) 0.00	2.57/4.65	2.53/5.69	0.73/6.72	0.00	2.57/4.65	2.53/5.69	0.73/6.72
	t(max) 0.82	4.10/3.33	——	——	8.43	10.5/53.0	——	——
	0.91	——	6.36/4.48	——	7.18	——	6.84/23.6	——
	2.69	——	——	5.58/3.22	0.25	——	——	1.38/6.75
	t(end) 1.47	0.061/4.40	——	——	497.8+	0.061/1744+	——	——
	1.47	——	0.061/3.10	——	223.9	——	0.061/322	——
	2.79	——	——	0.061/3.10	8.41	——	——	0.061/7.25
96.52	*t*(init) 0.00	1.47/4.65	3.29/5.69	2.18/6.72	0.00	1.47/4.65	3.29/5.69	2.18/6.72
	t(max) 0.69	4.87/3.86	——	——	13.82	11.09/91.5	——	——
	0.99	——	6.43/3.97	——	6.53	——	7.65/25.0	——
	1.48	——	——	6.37/5.13	0.84	——	——	3.19/7.17
	t(end) 1.03	0.061/3.54	——	——	486.2+	0.061/2077+	——	——
	1.35	——	0.061/3.33	——	486.2	——	0.061/2077	——
	2.21	——	——	0.0612/3.25	109.4	——	——	0.061/21.7

Table 2b *R* and *YR* as a function of time, axial distance, and starting circumferential angles 135 and 45 deg

			135 deg				45 deg	
Z/angle, ft	Second	*R*1/*YR*1, μm/ft	*R*2/*YR*2, μm/ft	*R*3/*YR*3, μm/ft	Second	*R*1/*TR*1, μm/ft	*R*2/*YR*2, μm/ft	*R*3/*YR*3, μm/ft
36.23	*t*(init) 0.00	1.28/4.65	——	——	0.00	1.28/4.65	——	——
	t(max) 25.84	15.8/321	——	——	3.85	2.10/5.42	——	——
	t(end) 495.8+	0.061/6036+	——	——	25.38	0.061/7.75	——	——
56.23	*t*(init) 0.00	2.52/4.65	1.22/5.69	——	0.00	2.52/4.65	1.22/5.69	——
	t(max) 0.00	2.52/4.65	——	——	8.52	9.23/42.1	——	——
	18.34	——	16.9/244	——	0.42	——	1.89/5.75	——
	t(end) 1.78	0.061/3.32	——	——	401.1	0.061/1041	——	——
	488+	——	0.061/7070+	——	99.79	——	0.061/7.83	——
75.22	*t*(init) 0.00	2.57/4.65	2.53/5.69	0.73/6.72	0.00	2.57/4.65	2.53/5.69	0.73/6.72
	t(max) 0.35	5.26/4.37	——	——	8.25	11.1/55.1	——	——
	22.7	——	17.2/325	——	7.73	——	7.39/26.6	——
	22.7	——	——	16.4/204	0.22	——	——	1.38/6.74
	t(end) 1.36	0.061/3.38	——	——	251.6+	0.061/1516+	——	——
	499.4+	——	0.061/7512+	——	251.6	——	0.061/437	——
	499.4	——	——	0.061/6658	8.36	——	——	0.061/7.10
96.52	*t*(init) 0.00	1.47/4.65	3.29/5.69	2.18/6.72	0.00	1.47/4.65	3.29/5.69	2.18/6.72
	t(max) 0.43	4.88/4.39	——	——	15.7	11.6/113	——	——
	20.46	——	15.8/254	——	8.58	——	8.25/34.4	——
	20.46	——	——	17.3/289	1.11	——	——	——
	t(end) 3.45	0.061/3.62	——	——	500+	0.061/2505+	——	——
	497.5+	——	0.061/6064+	——	319.4	——	0.061/679	——
	497.5+	——	——	0.061/7579	224.7	——	——	0.061/20.3

Table 2c *R* and *YR* as a function of time, axial distance, and starting circumferential angle 90 deg

Z/angle, ft	Second	*R*1/*YR*1, μm/ft	90 deg *R*2/*YR*2, μm/ft	*R*3/*YR*3, μm/ft
36.23	*t*(init) 0.00	1.28/4.65	——	——
	t(max) 10.13	2.62/5.81	——	——
	t(end) 42.6	0.061/11.1	——	——
56.23	*t*(init) 0.00	2.52/4.65	1.22/5.69	——
	t(max) 13.6	12.1/104	——	——
	11.2	——	2.50/6.49	——
	t(end) 500+	0.061/2862+	——	——
	40.1	——	0.061/10.7	——
75.22	*t*(init) 0.00	2.57/4.65	2.53/5.69	0.73/6.72
	t(max) 13.0	14.1/132	——	——
	8.44	——	10.0/40.9	——
	0.66	——	——	1.34/6.72
	t(end) 483+	0.061/4395+	——	——
	483	——	0.061/1471	——
	8.44	——	——	0.061/6.74
96.52	*t*(init) 0.00	1.47/4.65	3.29/5.69	2.18/6.72
	t(max) 18.9	14.3/202	——	——
	14.3	——	10.7/83.1	——
	1.25	——	——	3.20/6.76
	t(end) 198+	0.061/2247+	——	——
	198+	——	0.061/1155+	——
	49.8	——	——	0.061/16.4

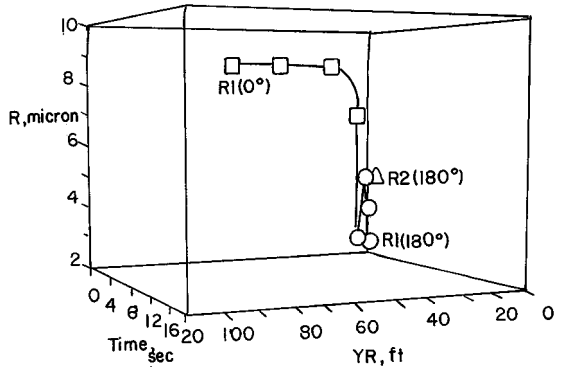

Fig. 5 Predicted droplet mean radius as a function of *YR* (starting at 4.65 and 5.69 ft), time, and starting circumferential angles (0 and 180 deg) at an axial distance of 56.23 ft.

135 deg

At the 36.23-ft axial distance and the *YR* streamline of 4.65 ft, the droplets grow to a maximum size and evaporate far outside of the plume and have rained out. At all of the other greater axial lengths, at the same *YR*, the droplet growth and evaporation patterns are the same as for the 180-deg case, i.e., they grow and evaporate to the nucleus toward the center of the plume. For all other outer *YR* streamlines the droplets grow to maximum size and evaporate far removed from the plume, i.e., they rain out. For the axial distance of 96.52 ft, Fig. 6 illustrates this behavior.

An examination of Tables 2a–2c, and as illustrated by Fig. 7 for the axial distance of 56.23 ft, shows the *YR* trajectories of droplets crossing those of other *YR* droplets, which is because of these droplets growing to a larger diameter and settling by gravity faster than the other droplets.

Effect of View Angle

Z = 36.23 ft

Looking down the vertical axis, i.e., 180–0 deg, the contrail thins rapidly by 1.65 s and disappears by 23.7 s. It deepens from a radius of 4.65 to 7.85 ft during this period. At the 135- to 45-deg view the contrail stretches to a radius of 7.75 ft and has dissipated by 25.4 s.

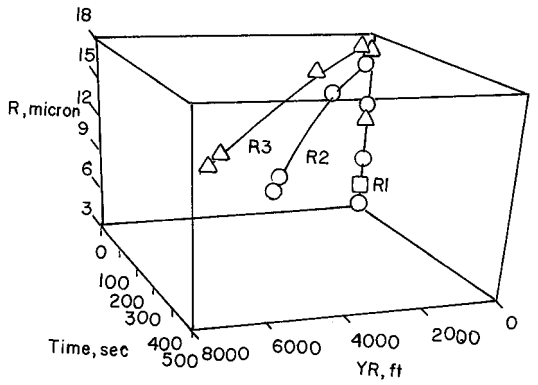

Fig. 6 Predicted droplet mean radius as a function of *YR* (starting at 4.65, 5.69, and 6.72 ft) and time, at a starting circumferential angle of 135 deg and an axial distance of 96.52 ft.

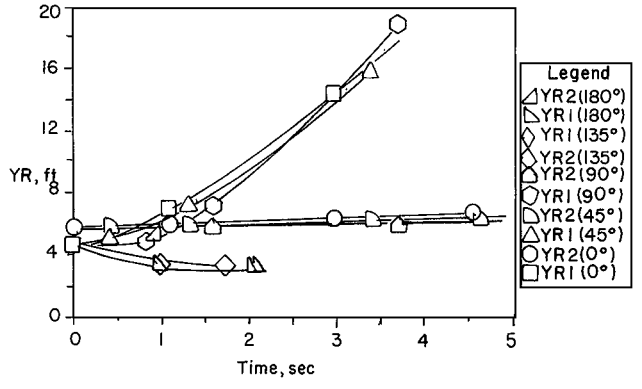

Fig. 7 Predicted *YR* location vs time, starting *YR* locations (4.65 and 5.69 ft), and circumferential angles (0, 45, 90, 135, and 180 deg) at an axial distance of 56.23 ft.

The droplets starting at 4.65 ft and 135 deg have rained out of the contrail before having evaporated. The droplets from 4.65 ft and 45 deg evaporate within the contrail. At 90 deg the contrail persists out to a radial distance of 11.1 ft and 42.6 s. In the broadest sense the contrail at this axial position persists for 23.7–42.6 s out to 11.1 ft in the vertical direction.

Z = 56.23 ft

At the 180- to 0-deg view, the contrail has dissipated by 32.8 s and spread down to a radius of 7.97 ft. It has already thinned materially by 2 s. The droplets starting at a *YR* of 4.65 ft either rain out or evaporate. It is the droplets from a starting *YR* of 5.69 ft that persist. For the 135–45 view, the contrail lasts until 99.8 s and is extended to a radius of 7.83 ft from the original *YR* of 5.69 ft but is thinned. For the 90-deg view the contrail persists for 40.1 s down to a radius of 10.67 ft for the droplets from the *YR* of 5.69 ft. The inner *YR* of 4.65 ft droplets are removed from the contrail by raining out. At this axial distance the contrail endures for 33–100 s at a maximum vertical radius of 10.7 ft.

Z = 75.22 ft

At the 180- to 0-deg axis, the droplets from the *YR* values of 4.65 and 5.69 ft have either rained out or have evaporated within the plume. The droplets from the *YR* of 6.72 ft last until 8.4 s to a radius of 7.25 ft. The droplets from the *YR* sites starting at 180 deg evaporate in 1.5 to 2.8 s. The 135- to 45-deg view indicates that the contrail persists to 7.1 ft and 8.4 s for the droplets from the original *YR* of 6.72 ft and 45 deg. The droplets from the 135-deg position either rain out or evaporate by 1.4 s. Finally, for the 90-deg view the contrail has disappeared after 8.4 s at a distance of 6.74 ft. The contrail at this axial distance persists for 8.4 s to a radial depth of 7.25 ft.

Z = 96.52 ft

The 180- to 0-deg view at this distance continues the trend just given. The deepest depth of the contrail is at 21.7 ft lasting for 109 s from the droplets starting at 0 deg and a *YR* of 6.72 ft. Droplets from the 180- deg start last 1.3 to 2.2 s to final *YR* values of 3.25 to 3.54 ft. The 135- to 45-deg view exhibits a contrail ranging to a depth of 20.28 ft for 225 s from the droplets starting at 45 deg. All other droplets from this position rain out of the plume. Droplets from the original *YR* of 4.65 ft and 135 deg last 3.5 s at a *YR* of 3.62 ft before evaporating. All other droplets rain out of the plume. At the 90-deg view the contrail lasts for 48.8 s to a radial distance of 16.37 ft. At this axial distance the maximum contrail depth is a radius of 20.3 ft persisting for 225 s.

Discussion

It is evident from these results that the contrail dissipation is quite complex, varying by the initial circumferential angle and streamline location, radially and axially. The contrail stretches vertically with time before disappearance; for this example, diffusion radially is negligible. The history of the contrail is dominated by gravity settling and the change in the plume temperature and condensable gas composition with time. The droplets that continue to grow outside the plume before evaporating can do so because they contain HCl, which depresses the vapor pressure of water in the droplet. Initially the droplets contain 9–20 wt % HCl; the concentration decreases to about 3 wt % by the time they evaporate completely. After radial distances of perhaps 20 ft, it is not likely that the contrail would persist because atmospheric winds and turbulence would disperse the droplet cloud.

The choice of 20 increments for the relaxation computation was a compromise between accuracy and computer limitations. Judging from the results obtained for the 20 increment calculation, however, not much would be gained by significantly increasing the number of increments.

In almost all cases the droplets grew to uniform size in a very short time. The Stokes settling velocity calculation was based therefore on the mean droplet diameter. In a few instances there was a nonuniform size distribution for a longer time interval, and this introduced some error in the computation.

Droplet agglomeration was not included in the computations. As illustrated by Fig. 6, clouds of droplets passed through other clouds of droplets within the contrail. Referring to Friedlander[11] and Reist,[12] the number of droplets collected by the large droplets falling through a cloud of smaller droplets can be expressed by

$$N = \pi\varepsilon(R_1 + R_2)^2(v_1 - v_2)c_1c_2 \qquad (6)$$

The plume contained initially, at any streamline, approximately 20,000 droplets per cc. Taking the case of a 10-μm radius droplet cloud falling through an 0.1-μm cloud of droplets by Stokes settling, the decrease in the number of 0.1-μm droplets is estimated to be approximately 15 droplets per second assuming a capture coefficient of 0.01—not significant for the times involved.

The case of the 10-μm cloud falling through a 5-μm cloud, as another example, cannot be predicted as well as for the preceding case because of the distortion of the flowfields around the larger droplets. It is expected that the capture coefficient for this larger 5-μm droplet would be less than for the 0.1-μm droplets. Using a capture coefficient of 0.01 nevertheless, the number of 5-μm droplets captured is estimated to be about 25 droplets per second—still not significant for the contact times and number of droplets in the clouds involved. Any agglomeration however would lead to decreased persistence of the contrail.

The model of the dissipation of the contrail of a typical reduced-smoke propellant rocket described here is equally applicable to one from a minimum-smoke propellant rocket. The absence of HCl in the plume of the latter rocket will change some of the details of the contrail dissipation, but the basic importance of Stokes settling and the change in the plume temperature and condensable gas composition with time will remain.

Conclusions

A model, CONDIS, has been presented that describes the dissipation of a solid-propellant rocket contrail comprised of secondary smoke of droplets of water or water-HCl. The history of the droplet evolution is dependent on the change in the gas composition and temperature with time by diffusion and by gravity settling of the droplets. The droplets first grow by condensation and then evaporate. Depending on the radial and axial location of the droplets, these occur within or far from the original plume radial dimensions. The contrail dimensions change vertically rather than radially because diffusion of the droplets radially is negligible compared with gravity settling. Agglomeration of the droplets is not important for this example. The contrail does not dissipate uniformly, but is highly dependent on its axial and radial location.

References

[1]Oliver, R. C., "Smokeless Solid Propellants: An Overview," Inst. for Defense Analysis, TDA RP 472, Arlington, VA, March 1969.

[2]Miller, E., "Smokeless Propellants," *Fundamentals of Solid-Propellant Combustion*, edited by K. K. Kuo and M. Summerfield , Vol. 90, Progress in Astronautics and Aeronautics, AIAA, New York, 1984, pp. 841–884.

[3]Miller, E., "Comparison of Experimental and Predicted Secondary Smoke Optical Signal Attenuation," *JANNAF 13th Plume Technology Meeting*, CPIA Pub. 357, Vol. 1, Chemical Propulsion Information Agency, Johns Hopkins Univ., Applied Physics Lab., Laurel, MD, 1982, pp. 451–458.

[4]Miller, E., "Prediction of the Visible Signature of Solid Rocket Plumes," *Journal of Spacecraft and Rockets*, Vol. 27, No. 1, 1990, pp. 82–84.

[5]Hoshizaki, H., Chou, Y. S., Myer, J. W., Wilson, K. H., and Thomas, P. D., "Plume Visibility Detection Study," Lockheed Palo Alto Research Labs., AFRPLTR-78-32, Vol. 1, Palo Alto, CA, Nov. 1978.

[6]Victor, A. C., and Breil, S. H., "A Simple Method for Predicting Rocket Exhaust Smoke Visibility," *Journal of Spacecraft and Rockets*, Vol. 14, No. 9, 1977, pp. 526–533.

[7]Victor, A. C., "Effects of Multiple Scattering on Rocket Exhaust Plume Smoke Visibility," *Journal of Spacecraft and Rockets*, Vol. 26, No. 4, 1989, pp. 274–278.

[8]Mikatarian, R. R., Kau, C. J., and Pergament, H. S., "A Fast Computer Program for Nonequilibrium Plume Predictions," AeroChem Research Lab., AFRPLTR-72-94, Princeton, NJ, Aug. 1972.

[9]Ranz, W. E., and Marshall, W. R., Jr., "Evaporation from Drops," *Chemical Engineering Progress*, Vol. 48, No. 3, 1952, pp. 141–146; also No. 4, pp. 173–180.

[10]Jakob, M., *Heat Transfer*, Vol. 1, Wiley, New York, 1949, pp. 377–379.

[11]Friedlander, S. K., *Smoke, Dust and Haze*, Wiley, New York, 1977, pp. 192–194.

[12]Reist, P. C., *Aerosol Science and Technology*, 2nd ed., McGraw–Hill, New York, 1993, pp. 314–316.